Dear Author

Here are the proofs of your article.

- You can submit your corrections **online** or by **fax**.
- For **online** submission please insert your corrections in the online correction form. Always indicate the line number to which the correction refers.
- Please return your proof together with the permission to publish confirmation.
- For **fax** submission, please ensure that your corrections are clearly legible. Use a fine black pen and write the correction in the margin, not too close to the edge of the page.
- Remember to note the journal title, article number, and your name when sending your response via e-mail, fax or regular mail.
- **Check** the metadata sheet to make sure that the header information, especially author names and the corresponding affiliations are correctly shown.
- **Check** the questions that may have arisen during copy editing and insert your answers/corrections.
- **Check** that the text is complete and that all figures, tables and their legends are included. Also check the accuracy of special characters, equations, and electronic supplementary material if applicable. If necessary refer to the *Edited manuscript*.
- The publication of inaccurate data such as dosages and units can have serious consequences. Please take particular care that all such details are correct.
- Please **do not** make changes that involve only matters of style. We have generally introduced forms that follow the journal's style.
  Substantial changes in content, e.g., new results, corrected values, title and authorship are not allowed without the approval of the responsible editor. In such a case, please contact the Editorial Office and return his/her consent together with the proof.
- If we do not receive your corrections **within 48 hours**, we will send you a reminder.

Please note

Your article will be published **Online First** approximately one week after receipt of your corrected proofs. This is the **official first publication** citable with the DOI. **Further changes are, therefore, not possible.**

After online publication, subscribers (personal/institutional) to this journal will have access to the complete article via the DOI using the URL:

`http://dx.doi.org/10.1007/s11581-021-04075-0`

If you would like to know when your article has been published online, take advantage of our free alert service. For registration and further information, go to: http://www.springerlink.com.

Due to the electronic nature of the procedure, the manuscript and the original figures will only be returned to you on special request. When you return your corrections, please inform us, if you would like to have these documents returned.

The **printed version** will follow in a forthcoming issue.

AUTHOR'S PROOF!

Metadata of the article that will be visualized in OnlineFirst

1	Article Title	**Nano α-Fe_2O_3 synthesized using EDTA-aqueous solution simple and novel method: improved capacity retention at 1 C rate as anode for high rate performance of lithium-ion batteries**	
2	Article Sub- Title		
3	Article Copyright - Year	**Springer-Verlag GmbH Germany, part of Springer Nature 2021 (This will be the copyright line in the final PDF)**	
4	Journal Name	Ionics	
5	Corresponding Author	Family Name	**Masoud**
6		Particle	
7		Given Name	**Emad M.**
8		Suffix	
9		Organization	Islamic University of Madinah
10		Division	Chemistry Department, Faculty of Science
11		Address	Madinah 20012, Saudi Arabia
12		Organization	Benha University
13		Division	Chemistry Department, Faculty of Science
14		Address	Benha 13518, Egypt
15		e-mail	emad.youssef@iu.edu.sa
16	Schedule	Received	23 February 2021
17		Revised	12 April 2021
18		Accepted	23 April 2021
19	Abstract	Depending on different preparation methods, two samples of nano α- Fe_2O_3, in addition to the commercial one, having different structural properties were successfully synthesized. All samples were characterized using different techniques such as X-ray diffraction (XRD), energy dispersive X-ray spectroscopy (EDX), infra-red spectroscopy (IR), scanning electron microscopy (SEM), Brunauer – Emmett – Teller (BET) nitrogen adsorption-desorption isotherm, and a vibrating sample magnetometer. All structural characterization parameters exhibited that the EDTA-prepared sample has the best textural structure, which support the electrochemical properties concerning the charge-discharge processes for the high rate performance of lithium-ion batteries. All results showed good anode electrochemical performance of EDTA-prepared sample at the high rates of 1 C and 2 C, especially the first electrochemical cycles of charge-discharge processes. A comparison with other recent previous related studies was performed to confirm the novelty and efficiency of EDTA-prepared sample for the high rate performance of lithium-ion batteries applications. **Graphical abstract:**	
20	Keywords separated	EDTA-prepared sample - High rate performance - Discharge capacity - Lithium	

	by ' - '	ion batteries - Energy storage
21	Foot note information	Springer Nature remains neutral with regard to jurisdictional claims in published maps and institutional affiliations.

Ionics
https://doi.org/10.1007/s11581-021-04075-0

ORIGINAL PAPER

Nano α-Fe_2O_3 synthesized using EDTA-aqueous solution simple and novel method: improved capacity retention at 1 C rate as anode for high rate performance of lithium-ion batteries

Emad M. Masoud [1,2]

Received: 23 February 2021 / Revised: 12 April 2021 / Accepted: 23 April 2021

Abstract

Depending on different preparation methods, two samples of nano α- Fe_2O_3, in addition to the commercial one, having different structural properties were successfully synthesized. All samples were characterized using different techniques such as X-ray diffraction (XRD), energy dispersive X-ray spectroscopy (EDX), infra-red spectroscopy (IR), scanning electron microscopy (SEM), Brunauer – Emmett – Teller (BET) nitrogen adsorption-desorption isotherm, and a vibrating sample magnetometer. All structural characterization parameters exhibited that the EDTA-prepared sample has the best textural structure, which support the electrochemical properties concerning the charge-discharge processes for the high rate performance of lithium-ion batteries. All results showed good anode electrochemical performance of EDTA-prepared sample at the high rates of 1 C and 2 C, especially the first electrochemical cycles of charge-discharge processes. A comparison with other recent previous related studies was performed to confirm the novelty and efficiency of EDTA-prepared sample for the high rate performance of lithium-ion batteries applications.

Keywords EDTA-prepared sample · High rate performance · Discharge capacity · Lithium ion batteries · Energy storage

Introduction

Many studies were recently devoted to nanostructured materials with different morphologies in the field of lithium-ion batteries (LIBs). Due to their high Li^+ diffusion coefficients and also the large contact area between the electrode and electrolyte, they can quickly absorb and store vast numbers of lithium ions without causing any deterioration in the electrode, and have better rate capability than conventional micron-scale materials [1–4]. Because of its low cost and raw materials abundance in nature, Fe_2O_3 has been used in many application fields such as lithium ion storage, gas sensors, catalysts, and magnetic applications [5–10]. The Fe_2O_3 crystal lattice can store six Li^+ per formula unit, and the theoretical capacity of Fe_2O_3 is as high as 1005 mAh/g, which is much higher than that of commercial graphite anode materials (372 mAh/g). Thus, the investigation of Fe_2O_3 as a lithium ion storage material should be potentially important in the search for new anode materials with high capacity for lithium-ion batteries [11–15]. Great efforts have been focused on the properties and preparation of hematite nanomaterials with controllable size and shape [16], such as nanocrystals [17], nanoparticles [18], nanocuboids [19], nanospindles [20], nanoflakes [21], nanorods [22], nanowires [23], nanobelts [24], and nanotubes [25]. Several methods, such as a template method [26], a sol-gel strategy [22], gas-solid reaction techniques [27], and a hydrothermal approach [25, 28], have been developed for the synthesis of hematite nanostructures. However, and till now, the rapid capacity fading, especially the initial capacity cycles and low cycle life stability behavior at high rates, attributed to the kinetic limitation and large volume change of α-Fe_2O_3 during the charge/discharge process present great challenge to the practical application of this material [29–31]. There are issues associated with the wet-chemistry methods for synthesizing these nanostructured materials, such as complex time consuming steps, high energy consumption, and difficulties in scaling up. In this paper, a

✉ Emad M. Masoud
emad.youssef@fsc.bu.edu.eg; emad_masoud1981@yahoo.com; emad.youssef@iu.edu.sa

[1] Chemistry Department, Faculty of Science, Benha University, Benha 13518, Egypt

[2] Chemistry Department, Faculty of Science, Islamic University of Madinah, Madinah 20012, Saudi Arabia

new trial to find a suitable and simple method giving nano-structured α- Fe_2O_3 particles and achieving the good initial capacity and cycle life stability at high rates, to resolve the problems of this material. In this vein, two simple methods were used to synthesize α- Fe_2O_3, in addition to a commercial sample, to study the effect of structural properties on the initial capacities through charge-discharge processes of this material at 1 C rate.

Experimental

Synthesis

Ferric chloride (99.9%, Sigma-Aldrich), ferric nitrate nonahydrate (99.9%, Sigma-Aldrich), EDTA (99.9%, Sigma-Aldrich), and urea (99.9%, Sigma-Aldrich) were used as starting materials, and as received without further purification for the two samples synthesis.

For the first method, α- Fe_2O_3 was synthesized via a hydrothermal process. Appropriate amounts of iron chloride and urea were dissolved in distilled water. The solution was sealed in a 30-ml Teflon-lined stainless steel autoclave and kept at 120 °C for 10 h. The precipitate was washed three times with distilled water and ethanol, and then dried in vacuum oven at 50 °C overnight. Following, the dried sample was calcined at 500 °C for 2 h.

For the second method, appropriate amount of ferric nitrate was dissolved in distilled water and mixed with aqueous solution of EDTA. The resulting mixture was stirred for 1 h at room temperature. Following, the mixture was evaporated on a hot plate, and a dark brown fluffy precursor was formed. After that, the precursor was grinded and calcined, in air, at 450 °C for 3 h at a heating rate of 2 °C/min.

The two synthesized samples, in addition to a commercial one, were denoted as S0, S1, and S2 for the commercial, urea-prepared (first method), and EDTA-prepared (second method) samples, respectively.

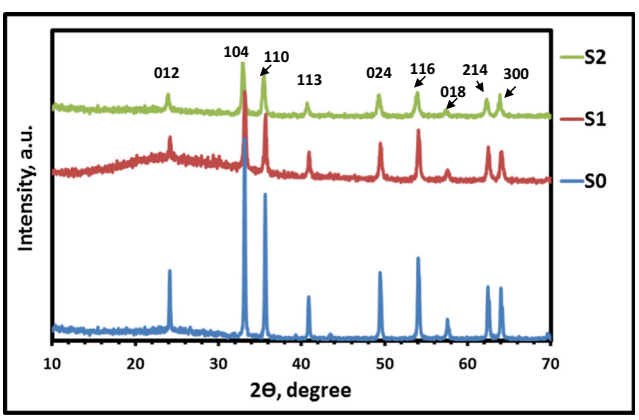

Fig. 1 XRD patterns of S0, S1, and S2 samples

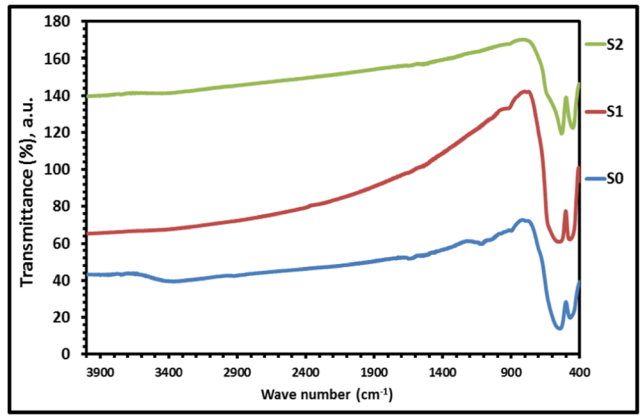

Fig. 2 FT-IR patterns of S0, S1, and S2 samples

Characterization

X-ray diffraction analysis was performed on a Diano (made by Diano Corporation, USA) with Cu-filtered CuKα radiation (λ = 1.5418 Å) energized at 45 kV, and 10 mA. The sample was measured at room temperature in the range from 2θ = 10 to 70°. The XRD phases present in the sample were identified with the help of ASTM Powder Data Files. The infrared spectra of the sample were recorded in the range of 300–3900 cm^{-1} using a Brucker-FTIR. The morphology of samples was examined using field emission scanning electron microscope (SEM, JEOL) operated at an accelerating voltage of 200 KV. The energy dispersive X-ray spectra (EDX) acquired during the SEM imaging. Surface area and porosity of the sample was determined by measuring Brunauer – Emmett – Teller (BET) nitrogen adsorption-desorption isotherm using volumetric method with a Micrometrics ASAP2020 apparatus. The magnetic properties were measured using a vibrating sample magnetometer (VSM; Lake Shore 7404).

Electrochemical measurements

For setting up the experimental cell of each sample, Fe_2O_3 powder (75 wt.%) was mixed with carbon black (10 wt.%), graphite (10 wt.%), and PVDF (5 wt.%) in presence of n-methylpyrrolidinone to make the mixture homogeneous and then the mixture was left on a hot plate for 3 h to evaporate the homogeneity material. After that, a certain weight of the powder was coated onto a cupper foil and some drops of n-methylpyrrolidinone were added again and then the powder

Table 1 Wave number values of the two basic stretching vibrational modes bands of Fe-O

Sample	Wave number values (cm^{-1}) of the two basic stretching vibrational modes bands of Fe-O	
S0	469	544
S1	470	556
S2	450	531

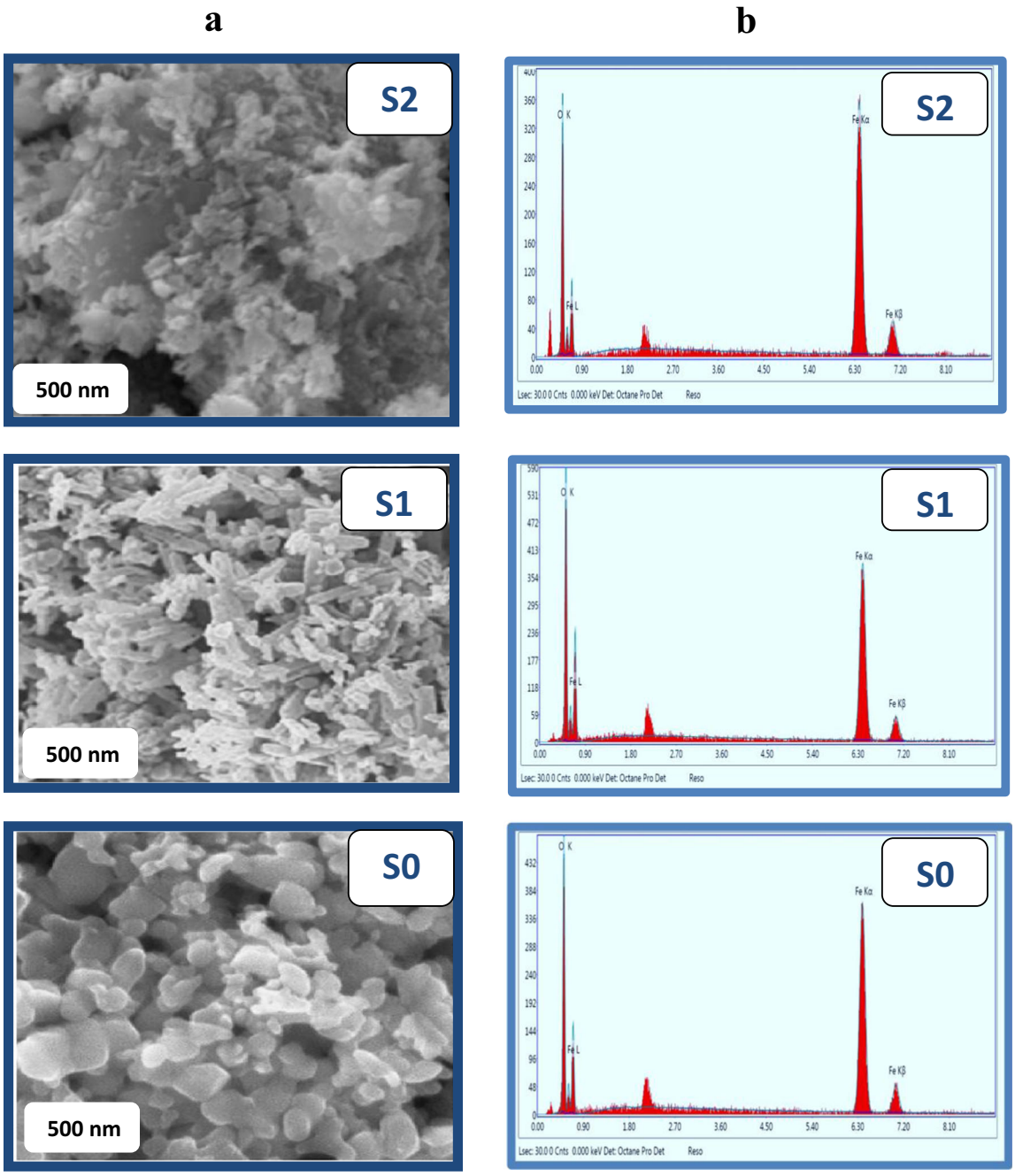

Q3 **Fig. 3** **a** SEM and **b** EDX patterns of S0, S1, and S2 samples

was dried under vacuum for 30 min at 120 °C. In a glove box under argon atmosphere, the cell was constructed as Swagelok cells. A porous polypropylene film was used for separating the cathode and a lithium metal anode, and a mixture of 1M $LiPF_6$-ethylene carbonate/dimethyl carbonate (1:1, v/v, Merck) was used as the electrolyte. The cells were galvanostatically charged and discharged using EG&G Electrochemical analyzer (Model – 6310) in the scan rate of

Table 2 Parameters values of N_2 adsorption/desorption isotherms and NLDFT/GCMC pore size distribution analysis of S0, S1, and S2 samples

Sample	Total pore volume (cm^3/g)	Mean pore diameter (nm)	W, peak (area) (nm)	V_p (cm^3/g)
S0	0.17	33.6	14.9	0.14
S1	0.11	77.6	24.6	0.095
S2	0.22	59.1	22.9	0.23

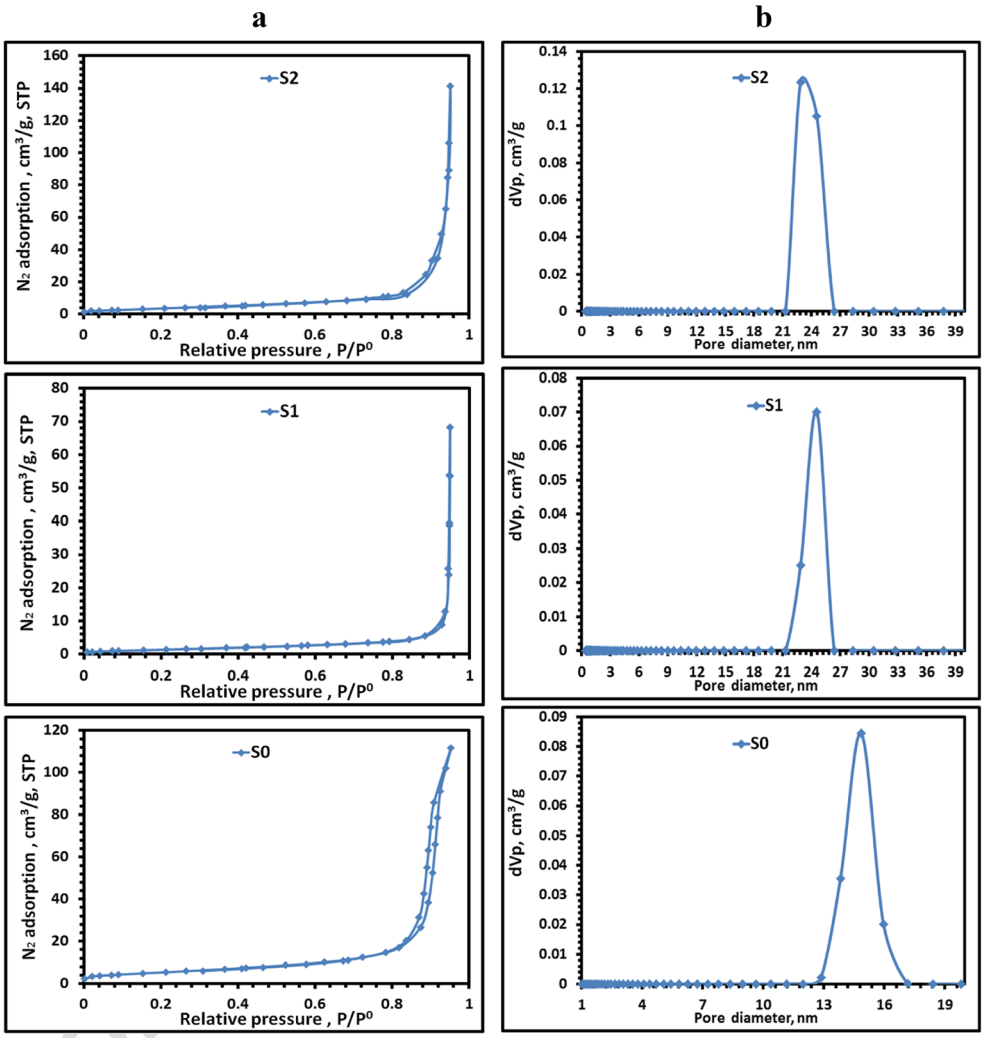

Fig. 4 **a** N_2 adsorption-desorption isotherms and **b** pore size distributions of S0, S1, and S2 samples

1 mVs^{-1} to perform charge-discharge processes for the assembled battery. The charge-discharge processes were performed at a voltage between 0 and 3 V and a rate of 1 C.

Results and discussion

The XRD patterns of S0, S1, and S2 are shown in Fig. 1. All patterns confirmed the crystal structure presence of standard hematite (a-Fe_2O_3) structure, JCPDS card No. 33-0664. Also, no impurity was detected indicating that all samples have a single-phase rhombohedral crystal structure. The particle size of all samples was calculated using the Scherer equation [32]. The S2 sample showed the smallest particle size (32 nm) compared to the other two ones that showed 230 nm and 70 nm for S0 and S1, respectively.

Figure 2 shows the FT-IR patterns of S0, S1, and S2 samples. The figure shows two strong bands in a region of 450–556 cm^{-1}. These bands relate to Fe-O stretching vibrational modes of α-Fe_2O_3 [33]. Other three small bands at around 3421 (for S0 sample), 1632 and 944 cm^{-1} (for all samples) can be assigned to stretching, wagging, and twisting vibrations of water molecules [34]. Moreover, some shifts of the two basic stretching vibrational modes bands of Fe-O were observed, Table 1. This shift can be attributed to particle size value difference of each sample which depends on the preparation method.

The SEM morphology of all samples is shown in Fig. 3a. It can be seen that the particle shape of S0 and S2 is not regular with high particles agglomeration. In contrast, the S1 sample showed a regular nanorods shape with low particles agglomeration. The nanorods diameters are in the range of 60–80 nm with a length of around 300–500 nm. The EDX spectra of all samples are also shown in Fig. 3b. All spectra confirmed the composition of nano α-Fe_2O_3.

The porous nanostructure of the S0, S1, and S2 samples was investigated using the N_2 adsorption-desorption measurement, Fig. 4(a, b). Figure 4a showed that all samples exhibit a typical type IV isotherm, indicating the existence of porous structure. The S2 sample showed the highest value of a total

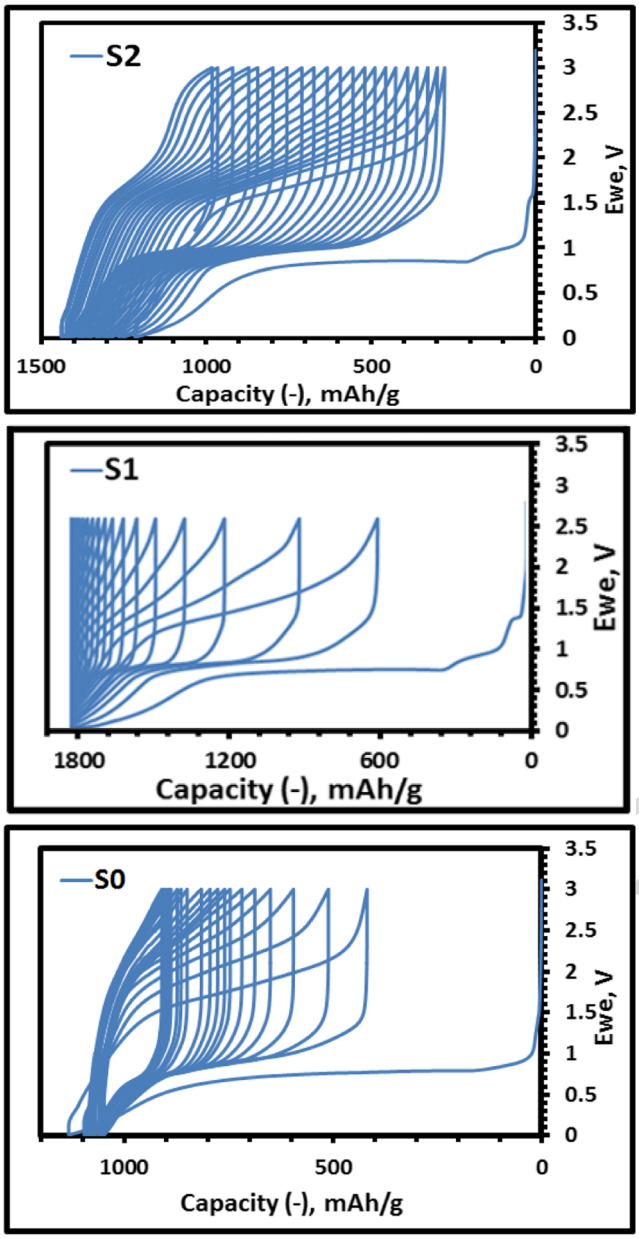

Fig. 5 Charge-discharge curves for S0, S1, and S2 samples between 0 and 3 V at 1 C rate

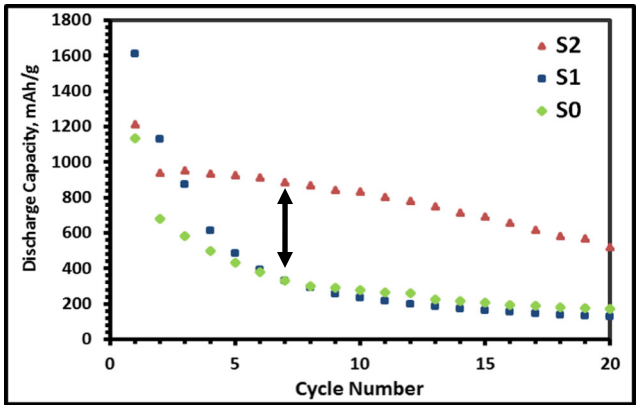

Fig. 6 Discharge capacity against cycle number for S0, S1, and S2 samples at 1 C rate

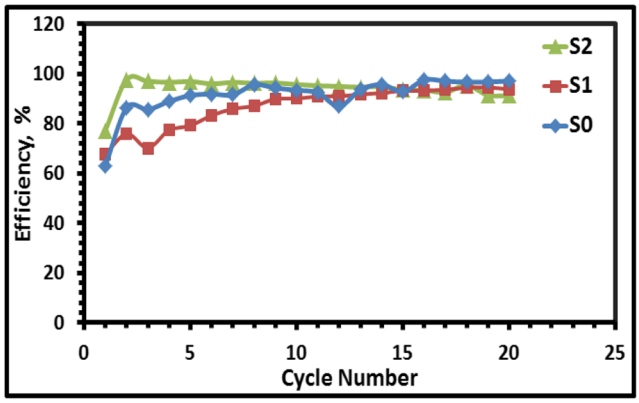

Fig. 7 Cycle number dependence of efficiency for S0, S1, and S2 samples at 1 C rate

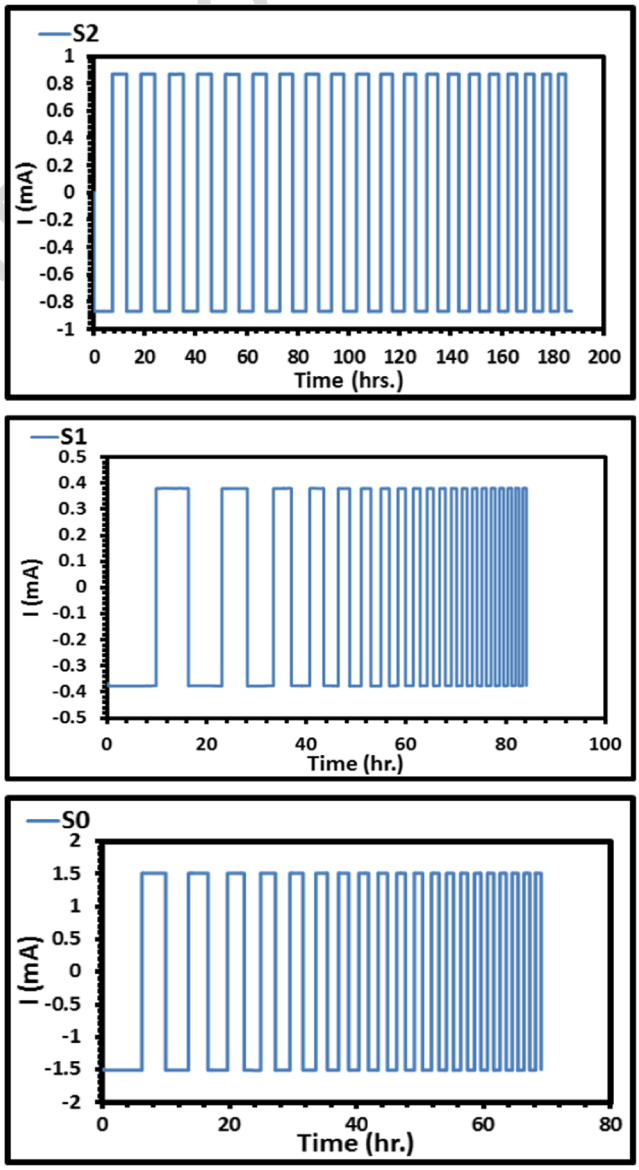

Fig. 8 Time dependence of current for S0, S1, and S2 sample at 1 C rate

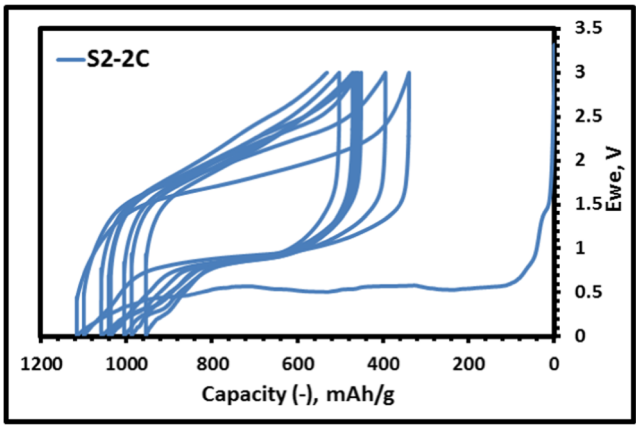

Fig. 9 Charge-discharge curves for S2 sample at 2 C rate

pore volume compared to the others ones, Table 2. In addition, the mean pore diameter of S1 sample showed the highest value compared to the others ones. In contrast, as shown in Fig. 4b (pore size distribution), the S2 sample showed the highest value of mesoporous diameter (22.9 nm) volume (0.23 cm^3/g) compared to the other ones. Overall, the results show that S2 sample has the best porous structure compared to the other ones. The mesoporous structure of S2 sample can be expected to possess the ability of liquid electrolyte holding and prevent the process of over-flooding through capillary force [35]. Thus, the mesoporous structure of S2 sample will play an important role in the electrochemical performance improvement of nano α-Fe_2O_3, specially for the high rates. Moreover, this porous structure can also decrease the volume variation of active material during electrochemical cycling, which is advantageous for the high performance rates. Additionally, from X-ray diffraction results, the same S2 sample showed the smallest particle size value (32 nm) which also will play a good role in reducing the mean Li ion diffusion pathways and increasing the contact surface area between the anode and the electrolyte as well [36]. These features of S2 sample will promote fast ionic transport and contribute to

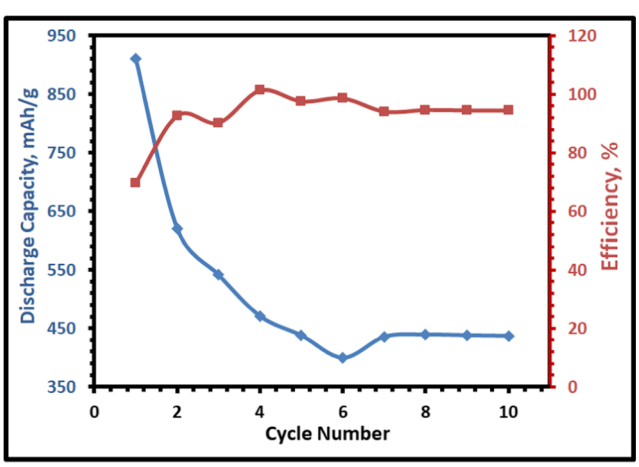

Fig. 10 Cycle number dependence of discharge capacity and efficiency for S2 sample at 2 C rate

Table 3 Magnetic properties of prepared samples at 298 K

Sample	Ms (emu/g)	Hc (G)	Mr (emu/g)
S0	0.91	72.6	22.79×10^{-3}
S1	0.62	550.3	99.42×10^{-3}
S2	1.15	538.8	0.215

faster charge-discharge processes, especially for the initial discharge processes of the high rates [37]. Figure 5 shows the charge-discharge curve for all cycles of S0, S1, and S2 samples at 1 C rate. The initial discharge curve of each sample shows a potential plateau at around 0.8 V (Li/Li^{+1}) followed by a sloping curve, which corresponds to the reduction reaction of nano α-Fe_2O_3. The sloping part, at the end of the discharge curve (between 0.4 and 0 V), is corresponding to the formation of a solid electrolyte interface layer [38, 39]. At the same time, the initial charge curve of each sample exhibits two slops a round 1.6 and 2.3 V in each charge curve which corresponding to the dissolution of the organic solid electrolyte interface layer [40, 41] and the charge reaction of nano α-Fe_2O_3, respectively. The observed main difference between the three samples is that the features of the charge-discharge curves of S0 and S1 samples starting from the 7th cycle are different about what was observed for S2 sample. This difference can be attributed to the decrease of the capacity values which is due to oxidation-reduction reaction low efficiency for the two samples compared to the other one. In order to show and prove this difference, values of discharge capacity against number of cycles for all samples were studied and shown in Fig. 6. The figure showed that the three samples have high initial discharge capacity values (1133 mAh/g for S0, 1610 mAh/g for S1, 1212 mAh/g for S2), but do not have the same decrease rate. The last discharge capacity values (174 mAh/g for S0, 128 mAh/g for S1, 520 mAh/g for S2) exhibited that S2 sample has the highest cyclability behavior compared to the other ones. The difference between initial and last discharge capacity values of the three samples reflects the

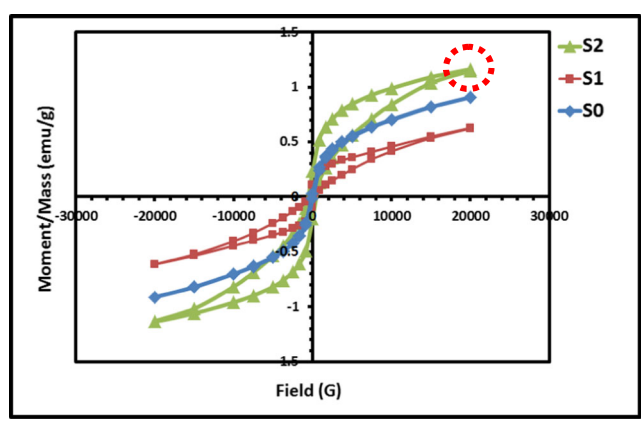

Fig. 11 Magnetic properties of S0, S1, and S2 samples

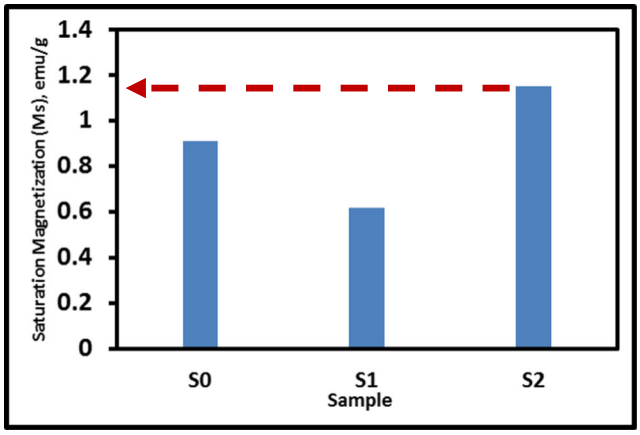

Fig. 12 Saturation magnetization (M_s) values of S0, S1, and S2 samples

difference of the curves features discussed above. The S2 sample, as expected above, showed the good cyclability behavior at 1 C rate compared to the other ones. The textural properties of this sample which demonstrate that pores ratio, mesoporous structure, and small particle size play a big role in enhancing the oxidation-reduction reactions of charge-discharge processes as discussed before. The coulomb efficiency behavior of S0, S1, and S2 samples through charge-discharge processes at 1 C rate were studied, Fig. 7. The figure exhibited that samples have the following order of initial cycle coulomb efficiency values [S2 (77%) > S1 (68%) > S0 (63%)], while the following order of last cycle ones [S0 (97%) > S1 (94%) > S2 (91%)]. This also shows that S2 sample has a good coulomb efficiency value through charge-discharge processes. The extra capacities can be attributed to the decomposition of non-aqueous electrolyte during the discharge process [40]. Figure 8 shows the charge-discharge current versus time for nano α-Fe_2O_3/ Li cell of all samples. The figures reflected the regular behavior of each sample for current change with time through all charge-discharge cycles. The area under lines of figures depicts the capacity retention, which reflects that S2 sample has the highest one compared to the others. For more investigation about the good performance of S2 sample at high rates, the charge-discharge curve for the first 10 cycles at 2 C rate was studied, Fig. 9. The figure showed the same behaviors observed before for the sample at 1 C rate. The discharge capacity values and the coulomb efficiency behavior of those cycles were shown in Fig. 10. The sample exhibited an initial discharge capacity of 915 mAh/g, and a last one of 450 mAh/g. This indicating that this sample also exhibits good capacity retention at this high rate and ensuring that it is a promised anode for the high rate performance of lithium ion batteries. The figure also exhibited that the sample has a coulomb efficiency of 70% for the first cycle, and 95% for the last one. This also ensure the good performance of S2 sample.

As magnetic properties are one of the most important ones that reflect the electrical and electrochemical behaviors, the magnetic curves of all prepared sampled were studied, Fig. 11. The various parameters (saturation magnetization (M_s), remanent (M_r), and coercivity (H_c)) were determined, Table 3. The observed results indicated that all samples have a ferromagnetic behavior with different values of magnetic parameters. The S2 sample showed the highest value of Ms compared to the others with the following order [S2 (Ms = 1.15 emu/g) > S0 (Ms = 0.91 emu/g) > S1 (Ms = 0.62 emu/g)], Fig. 12. In general, the difference of magnetic parameters values of all prepared samples can be attributed to the different preparation methods, which result in different particle size and morphology (as mentioned in details of structural characterization part). The highest value of M_s for S2 sample can be

Table 4 Comparison of the electrochemical properties of S2 sample with other previous studies

Sample	Particle size (nm)	Current density (C), (mA/g)	Potential range (V)	Initial discharge capacity ($mAhg^{-1}$)	Capacity retention ($mAhg^{-1}$)	References
S2	32 nm	1 C	0–3	1212	833 after 10 cycles	This work
		2 C	0–3	920	450 after 10 cycles	This work
Nano rods α-Fe_2O_3/40% conductive carbon	60-80 nm	0.1 C	0.01–3	1320	850 after 10 cycles	[43]
Nano α-Fe_2O_3 synthesized using PEG-600	700 nm (thickness)	20 mA/g	0.01–3	1248.1	750 after 10 cycles	[44]
Nano α-Fe_2O_3	Average diameter of 200 nm	1 C	0.01–3	1000	750 after 10 cycles	[45]
Ni-Co-doped Fe_2O_3	Microsphe-res	200 mA/g	0.01–3	1050	580 After 10 cycles	[46]
Fe_2O_3/CF	10 nm	50 mA/g	0.01–3	1680	780 After 10 cycles	[47]
Fe_2O_3	–	1 C	0.01–2.5	1200	200 After 10 cycles	[48]
α-Fe_2O_3	Sphere-like diameter 500 nm	0.1 C	0.01–3	920	720 After 10 cycles	[49]
α-Fe_2O_3/carbon aerogel	–	100 mA/g	0.1–3	850	600 After 10 cycles	[50]
α-Fe_2O_3	–	100 mA/g	0.1–3	1250	700 After 10 cycles	[50]

attributed to the small particle size of this sample [42] compared to the others.

To confirm the novelty and efficiency of nano α-Fe_2O_3 synthesized using EDTA-aqueous solution for the high rate performance of lithium ion batteries, a comparison with other previous studies of the same material at low and high rates was established and tabulated, Table 4. All results showed that nano α-Fe_2O_3 synthesized using EDTA-aqueous solution is a promised material for the lithium ion batteries application at high rates.

Conclusions

Urea-prepared (S1) and EDTA-prepared (S2) samples of nano α-Fe_2O_3 were synthesized, in addition to a commercial (S0) one. Different structural properties were obtained depending on the preparation method. The EDTA-prepared sample (S2) of nano α-Fe_2O_3 exhibited the smallest particle size compared to other samples, with high agglomeration irregular shape. The sample also showed the highest value of mesoporous diameter (22.9 nm) volume (0.23 cm^3/g) compared to the other ones. The electrochemical results of charge-discharge processes showed that the three samples have high initial discharge capacity values (1133 mAh/g for S0, 1610 mAh/g for S1, 1212 mAh/g for S2), but do not have the same decrease rate. The last discharge capacity values (174 mAh/g for S0, 128 mAh/g for S1, 520 mAh/g for S2) exhibited that S2 sample has the highest cyclability behavior compared to the other ones. Also, the samples exhibited the following order of initial cycle coulomb efficiency values [S2 (77 %) > S1 (68 %) > S0 (63 %)], while the following order of last cycle ones [S0 (97 %) > S1 (94 %) > S2 (91 %)]. This shows that S2 sample has a good coulomb efficiency value through charge-discharge processes. The good performance of S2 sample was also observed at 2 C rate. The magnetic properties showed the highest saturation magnetization (Ms) of S2 sample compared to the others. The novelty and efficiency of EDTA-prepared sample were also confirmed by a comparison with other related previous studies for the same material. All results exhibited that EDTA-prepared sample is a promised anode material for the high rate performance of lithium-ion batteries applications.

Acknowledgements I would like to thank the Science and Technology Development Fund (STDF), Egypt, (http://www.stdf.org.eg/index.php/en/) for the financial support of this scientific research work through Short –Term Fellowship (STF) project. Also, my sincere thanks to Prof. Dr. Xiangwu Zhang (College of textiles, North Carolina State University, USA) for his acceptance to perform a part of this work in his lab.

References

1. Mai L, Hu B, Chen W, Qi Y, Lao C, Yang R, Dai Y, Wang ZL (2007) Lithiated MoO_3 Nanobelts with greatly improved performance for lithium batteries. Adv Mater 19:3712–3716
2. Maier J (2005) Nanoionics: ion transport and electrochemical storage in confined systems. Nat Mater 4:805–815
3. Hu YS, Kienle L, Guo YG, Maier J (2006) High lithium electroactivity of nanometer-sized rutile TiO_2. Adv Mater 18: 1421–1426
4. Mai LQ, Chen W, Xu Q, Peng JF, Zhu QY (2003) Mo doped vanadium oxide nanotubes: microstructure and electrochemistry. Chem Phys Lett 382:307–312
5. Gou XL, Wang GX, Park JS, Liu H, Yang J (2008) Monodisperse hematite porous nanospheres: synthesis, characterization, and applications for gas sensors. Nanotechnology 19:125606
6. Teranishi T, Wachi A, Kanehara M, Shoji T, Sakuma N, Nakaya M (2008) Conversion of anisotropically phase-segregated Pd/γ-Fe2O3 nanoparticles into exchange-coupled fct-FePd/α-Fe Nanocomposite Magnets. J Am Chem Soc 130:4210–4211
7. Karunakaran C, Senthilvelan S (2006) Fe_2O_3-photocatalysis with sunlight and UV light: oxidation of aniline. Electrochem Commun 8:95–101
8. Wu CZ, Yin P, Zhu X, OuYang CZ, Xie Y (2006) Synthesis of hematite (α-Fe2O3) nanorods: diameter-size and shape effects on their applications in magnetism, lithium ion battery, and gas sensors. J Phys Chem B 110:17806–17812
9. Shekhah O, Ranke W, Schule A, Kolios G, Schlogl R (2003) Styrene synthesis: high conversion over unpromoted iron oxide catalysts under practical working conditions. Angew Chem Int Ed 42:5760–5763
10. Teng XW, Liang XY, Rahman S, Yang H (2005) Porous nanoparticle membranes: synthesis and application as fuel-cell catalysts. Adv Mater 17:2237–2241
11. Wang PC, Ding HP, Bark T, Chen CH (2007) Nanosized α-Fe_2O_3 and Li–Fe composite oxide electrodes for lithium-ion batteries. Electrochim Acta 52:6650–6655
12. Larcher D, Bonnin D, Cortes R, Rivals I, Personnaz L, Tarascon JM (2003) Combined XRD, EXAFS, and Mössbauer studies of the reduction by lithium of α Fe_2O_3 with various particle sizes. J Electrochem Soc 150:A1643
13. Larcher D, Masquelier C, Bonnin D, Chabre Y, Masson V, Leriche JB, Tarascon JM (2003) Effect of particle size on lithium intercalation into α Fe_2O_3. J Electrochem Soc 150:A133
14. Hibino M, Terashima J, Yao T (2007) Reversible and rapid discharge–charge performance of γ–Fe_2O_3 prepared by aqueous solution method as the cathode for lithium-ion battery. J Electrochem Soc 154:A1107
15. Zhou WW, Tang KB, Zeng SA, Qi YX (2008) Room temperature synthesis of rod-like $FeC_2O_4 \cdot 2H_2O$ and its transition to maghemite, magnetite and hematite nanorods through controlled thermal decomposition. Nanotechnology 19:065602
16. Sugimoto T, Sakata K (1992) Preparation of monodisperse pseudocubic α-Fe_2O_3 particles from condensed ferric hydroxide gel. J Colloid Interface Sci 152:587–590
17. Sun SH, Zeng H, Robinson DB, Raoux S, Rice PM, Wang SX, Li GX (2004) Monodisperse MFe_2O_4 (M = Fe, Co, Mn) Nanoparticles. J Am Chem Soc 126:273–279
18. Fadeev M, Kozlovskiy A, Korolkov I, Egizbek K, Nazarova A, Chudoba D, Rusakov V, Zdorovets M (2020) Iron oxide@ gold nanoparticles: synthesis, properties and potential use as anode materials for lithium-ion batteries. Colloids Surf A Physicochem Eng Asp 603:125178
19. Hamada S, Matijivic E (1981) Ferric hydrous oxide sols. IV. Preparation of uniform cubic hematite particles by hydrolysis of

ferric chloride in alcohol—water solutions. J Colloid Interface Sci 84:274–277
20. Ozaki M, Kratohvil S, Matijevic E (1984) Formation of monodispersed spindle-type hematite particles. J Colloid Interface Sci 102:146–151
21. Zhu YW, Yu T, Sow CH, Liu YJ, Wee ATS, Xu XJ, Lim CT, Thong JTL (2005) Efficient field emission from α-Fe_2O_3 nanoflakes on an atomic force microscope tip. Appl Phys Lett 87: 023103
22. Woo K, Lee HJ, Ahn JP, Park YS (2003) Sol–gel mediated synthesis of Fe_2O_3 nanorods. Adv Mater 15:1761–1764
23. Wang RM, Chen YF, Fu YY, Zhang H, Kisielowski C (2005) Bicrystalline hematite nanowires. J Phys Chem B 109:12245–12249
24. Wen XG, Wang SH, Ding Y, Wang ZL, Yang SH (2005) Controlled growth of large-area, uniform, vertically aligned arrays of α-Fe_2O_3 nanobelts and nanowires. J Phys Chem B 109:215–220
25. Liu H, Luo S h, Yan S x, Wang Q, Hu D b, Wang Y l, Feng J, FengYi T (2019) High-performance α-Fe_2O_3/C composite anodes for lithium-ion batteries synthesized by hydrothermal carbonization glucose method used pickled iron oxide red as raw material. Compos Part B 164:576–582
26. Chen J, Xu LN, Li WY, Gou XL (2005) α-Fe_2O_3 Nanotubes in gas sensor and lithium-ion battery applications. Adv Mater 17:582
27. Liu L, Kou HZ, Mo WL, Liu HJ, Wang YQ (2006) Surfactant-assisted synthesis of α-Fe_2O_3 nanotubes and nanorods with shape-dependent magnetic properties. J Phys Chem B 110: 15218–15223
28. Wan J, Chen X, Wang Z, Yang X, Qian YT (2005) A soft-template-assisted hydrothermal approach to single-crystal Fe3O4 nanorods. J Cryst Growth 276:571–576
29. Wang Z, Luan D, Madhavi S, Hu Y, Lou XWD (2012) Assembling carbon-coated α-Fe_2O_3 hollow nanohorns on the CNT backbone for superior lithium storage capability. Energy Environ Sci 5:5252–5256
30. Wang B, Chen JS, Wu HB, Wang ZY, Lou XW (2011) Quasiemulsion-templated formation of α-Fe_2O_3 hollow spheres with enhanced lithium storage properties. J Am Chem Soc 133: 17146–17148
31. Wang ZY, Luan DY, Madhavi S, Li CM, Lou XW (2011) α-Fe_2O_3 nanotubes with superior lithium storage capability. Chem Commun 47:8061–8063
32. Mahmoud WE, El-Mallah H (2009) Synthesis and characterization of PVP-capped CdSe nanoparticles embedded in PVA matrix for photovoltaic application. J Phys D Appl Phys 42:035502
33. Adegoke HI, AmooAdekola F, Fatoki OS, Ximba BJ (2013) Adsorption of Cr (VI) on synthetic hematite (α-Fe_2O_3) nanoparticles of different morphologies. Korean J Chem Eng 31:142–154
34. Barakat NAM, Khil MS, Sheikh FA, Kim HY (2008) Synthesis and optical properties of two cobalt oxides (CoO and Co_3O_4) nanofibers produced by electrospinning process. J Phys Chem C 112:12225–12233
35. Wu XH, Wu WW, Zhou Y, Huang XS, Chen W, Wang Q (2015) Synthesis and electrochemical performance of SnO_2–Fe_2O_3 composite as an anode material for Na-ion and Li-ion batteries. Powder Technol 280:119–123
36. Choi SH, Son JW, Yoon YS, Kim J (2006) Particle size effects on temperature-dependent performance of LiCoO2 in lithium batteries. Power Sour 158:1419
37. Tarascon JM, Armand M (2001) Issues and challenges facing rechargeable lithium batteries. Nature 414:359–367
38. Liu H, Wang GX, Liu J, Qiao SZ, Ahn H (2011) Highly ordered mesoporous NiO anode material for lithium ion batteries with an excellent electrochemical performance. J Mater Chem 21:3046
39. Kavitha T, Yuvaraj H (2011) A facile approach to the synthesis of high-quality NiO nanorods: electrochemical and antibacterial properties. J Mater Chem 21:15686
40. Grugeon S, Laruelle S, Herrera-Urbina R, Dupont L, Poizot P, Tarascon JM (2001) Particle size effects on the electrochemical performance of copper oxides toward lithium. J Electrochem Soc 148:A285
41. Debart A, Dupont L, Poizot P, Leriche J-B, Tarascon JM (2001) A transmission electron microscopy study of the reactivity mechanism of tailor-made CuO particles toward lithium. J Electrochem Soc 148:A1266
42. Lassoued A, Lassoued M, Dkhil B, Ammar S, Gadri A (2018) Synthesis, photoluminescence and magnetic properties of iron oxide (α-Fe_2O_3) nanoparticles through precipitation or hydrothermal methods. Phys E Low-dim Syst Nanostruct 101:212–219
43. Liu H, Wang G, Park J, Wang J, Liu H, Zhang C (2009) Electrochemical performance of α-Fe_2O_3 nanorods as anode material for lithium-ion cells. Electrochim Acta 54:1733–1736
44. Li YN, Zeng R, Zhang P, Guo Z, Liu H (2008) Controlled synthesis of α-Fe_2O_3 nanostructures and their size-dependent electrochemical properties for lithium-ion batteries. J Power Sources 184:456–461
45. Liu R, Zhang C, Wang Q, Shen C, Wang Y, Dong Y, Zhang N, Wu M (2018) Facile synthesis of α-Fe_2O_3@ C hollow spheres as ultra-long cycle performance anode materials for lithium ion battery. J Alloys Compd 742:490–496
46. Qi X, Yan Z, Liu Y, Li X, He G, Komarneni S (2018) Ni and Co doped yolk-shell type Fe_2O_3 hollow microspheres as anode materials for lithium-ion batteries. Mater Chem Phys 211:452–461
47. Sun C, Chen S, Li Z (2018) Controllable synthesis of Fe_2O_3-carbon fiber composites via a facile sol-gel route as anode materials for lithium ion batteries. Appl Surf Sci 427:476–484
48. Li H, Zhu X, Sitinamaluw H, Wasalathilak K, Xu L, Zhang S, Yan C (2017) Graphene oxide wrapped Fe_2O_3 as a durable anode material for high-performance lithium-ion batteries. J Alloys Compd 714:425–432
49. Yan Y, Tang H, Wu F, Xie Z, Xu S, Qu D, Wang R, Wu F, Pan M, Qu D (2017) Facile synthesis of Fe_2O_3@ graphite nanoparticle composite as the anode for lithium ion batteries with high cyclic stability. Electrochim Acta 253:104–113
50. Luo D, Lin F, Xiao W (2017) Wenjun Zhu, Synthesis and electrochemical performance of α-Fe_2O_3@ carbon aerogel composite as an anode material for Li-ion batteries. Ceram Int 43:2051–2056

AUTHOR QUERIES

AUTHOR PLEASE ANSWER ALL QUERIES.

Q1. The article title was slightly modified. Please check if appropriate.
Q2. Please check if the author details and the corresponding affiliations are presented correctly.
Q3. Figures 3, contains poor quality of text in image. Otherwise, please provide replacement figure file.